Nanoscale

PAPER

Cite this: *Nanoscale*, 2015, **7**, 17468

Monolayer-by-monolayer stacked pyramid-like MoS_2 nanodots on monolayered MoS_2 flakes with enhanced photoluminescence

Cailei Yuan,*[a] Yingjie Cao,[a] Xingfang Luo,*[a] Ting Yu,[a] Zhenping Huang,[b] Bo Xu,[b] Yong Yang,[a] Qinliang Li,[a] Gang Gu[a] and Wen Lei[c]

Received 8th August 2015,
Accepted 20th September 2015

DOI: 10.1039/c5nr05363c

www.rsc.org/nanoscale

The precise control of the morphology and crystal shape of MoS_2 nanostructures is of particular importance for their application in nanoelectronic and optoelectronic devices. Here, we describe a single step route for the synthesis of monolayer-by-monolayer stacked pyramid-like MoS_2 nanodots on monolayered MoS_2 flakes using a chemical vapor deposition method. First-principles calculations demonstrated that the bandgap of the pyramid-like MoS_2 nanodot is a direct bandgap. Enhanced local photoluminescence emission was observed in the pyramid-like MoS_2 nanodot, in comparison with monolayered MoS_2 flakes. The findings presented here provide new opportunities to tailor the physical properties of MoS_2 *via* morphology-controlled synthesis.

Introduction

Monolayered molybdenum disulfide (MoS_2), composed of three layers of atoms where Mo atoms are sandwiched between two layers of S atoms, has attracted much attention from researchers because of its direct bandgap electronic structure and unique excitonic properties.[1,2] In particular, MoS_2 in its monolayer form has broad applications in photonic devices,[3,4] including light-emitting devices,[5] photodetectors,[6] solar cells,[7] and so forth. The performances of these devices are determined by the physical properties of MoS_2 layered materials, which are, fundamentally, determined by the material characteristics, such as morphology and quality. So, it is essential to synthesize high quality MoS_2 films with the desired morphology and physical properties.[8] In general, the fabrication methods for monolayered MoS_2 flakes from bulk MoS_2 include mechanical exfoliation,[9] intercalation assisted exfoliation,[10,11] liquid exfoliation,[12] physical vapor deposition,[13] hydrothermal synthesis,[14] and thermolysis of the single precursor containing Mo and S.[15] Using these synthetic methods, relatively large-sized monolayered MoS_2 with a lateral dimension size up to submicron has been reported.

To develop high performance MoS_2-based photonic devices, the tunability of the optical properties of the material is important, such as photoluminescence (PL) emission. Currently, the PL emission of MoS_2 can be tuned in several ways, such as chemical doping,[16] electrical doping,[17] changing the temperature,[18] strain engineering,[19] alloying,[20] modification of interlayer coupling,[21] and so forth. It has also been demonstrated that the interplay between photogenerated carriers, excitons, and the surface acoustic wave (SAW) induced electro-acoustic field leads to strong dependence of the PL intensity on the SAW amplitude and excitation intensity.[22] However, another important approach to tune the optical properties is to utilize the quantum confinement effect, which can be achieved, for instance *via* reducing the material size from bulk to large area monolayer to nanodots.[23] However, most of the recent attention has been focused on the fabrication, property and application studies of MoS_2 flakes with the relevant exploration of MoS_2 nanodots being ignored, which present new physical properties and important device applications.

In this paper, we have demonstrated the growth of monolayer-by-monolayer stacked pyramid-like MoS_2 nanodots on monolayered MoS_2 flakes using a chemical vapor deposition (CVD) method. First-principles calculations demonstrated that the bandgap of the pyramid-like MoS_2 nanodot is a direct bandgap. Because of the significant enhancement of the PL efficiency caused by the monolayers of pyramid-like MoS_2 nanodots, strong PL enhancement was observed from this unique morphology of MoS_2 nanostructures. The findings

[a]*Jiangxi Key Laboratory of Nanomaterials and Sensors, Jiangxi Key Laboratory of Photoelectronics and Telecommunication, School of Physics, Communication and Electronics, Jiangxi Normal University, Nanchang 330022, Jiangxi, China. E-mail: clyuan@jxnu.edu.cn, xfluo@jxnu.edu.cn*
[b]*School of Physics, Communication and Electronics, Jiangxi Normal University, Nanchang 330022, Jiangxi, China*
[c]*School of Electrical, Electronic and Computer Engineering, University of Western Australia, Crawley, WA 6009, Australia*

presented here bring new opportunities to engineer the properties of MoS_2 *via* morphology-controlled synthesis.

Experimental

Pyramid-like MoS_2 nanodots on monolayered MoS_2 flakes were fabricated *via* a one-step approach with the CVD method. A two temperature zone tube furnace was used to provide accurate temperature control of the solid MoO_3 and sulfur (S), respectively. An alumina boat with S powders (99.9% purity) was placed upstream in the low-temperature zone. Another alumina boat containing MoO_3 (99.9% purity) was placed downstream in the high-temperature zone. A piece of Si wafer with a 300 nm SiO_2 layer substrate was placed face down to the MoO_3 powder. The distance between these two alumina boats is 14 cm. The temperature of S and the substrate was increased concurrently to 200 °C and 750 °C under an Ar flow, respectively. The sample was synthesized by evaporating S and MoO_3 powders simultaneously with a stoichiometric Mo to S ratio of 4 : 1 at an Ar flow rate of 30 sccm. After 3 minutes, the furnace was cooled down naturally to room temperature. The morphology of the MoS_2 nanostructures was examined by using Park system atomic force microscopy (AFM). The crystal structure and quality of MoS_2 nanostructures were examined by using a Rigaku X-ray diffractometer (XRD) with Cu Kα radiation. Raman spectra were recorded by using a Horiba Jobin Yvon Raman microscopic system. The solid-state excitation laser has a wavelength of 532 nm, and the laser spot size was 1 μm in diameter and a 100× objective was used to focus the laser beam. The PL measurements were also performed with the same laser by using the PL mode of the Raman microscopic system.

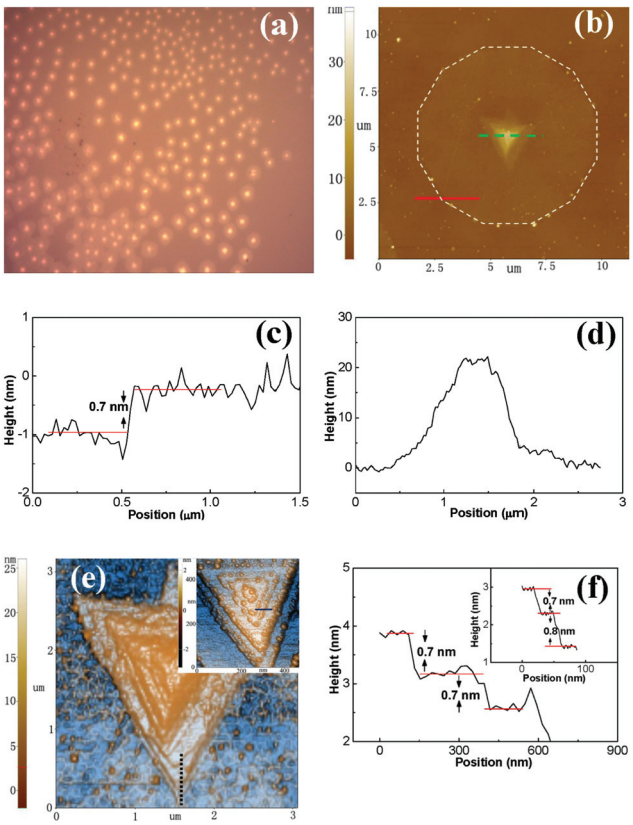

Fig. 1 (a) Optical microscopy image of MoS_2 flakes deposited on the SiO_2/Si substrate; (b) a typical AFM image of the MoS_2 flake; (c) height profile of the MoS_2 flake; (d) height profile of a pyramid-like MoS_2 nanodot; (e) side view of the high resolution AFM image of a pyramid-like MoS_2 nanodot; the top view of the high resolution AFM image of a pyramid-like MoS_2 nanodot in the top right corner; (f) step height profile of the corresponding region of the side viewed MoS_2 nanodot; step height profile of the corresponding region of the top viewed MoS_2 nanodot in the top right corner.

Results and discussion

Fig. 1(a) shows the optical microscopy image of MoS_2 flakes synthesized on the SiO_2/Si substrate with a pure Ar carrier gas flow rate of 30 sccm. The brighter-contrast flakes on the surface indicate the MoS_2 flakes, and the surrounding regions correspond to the SiO_2/Si substrate. A high density of flakes with a fairly uniform lateral size is formed over the surface of the substrate. Most importantly, it can be found that there is a shining spot on every MoS_2 flake and the thicknesses of these spots decrease from centers to edges. In order to further confirm the morphology and thickness of these MoS_2 flakes, AFM was used to examine the MoS_2 flakes. Fig. 1(b) illustrates the AFM image of a representative MoS_2 flake. The smooth surface morphology of the MoS_2 flake can be observed clearly, suggesting that the one layered structure of MoS_2 is formed. The MoS_2 flake has a dodecagonal shape, which corresponds to the Mo-rich conditions.[24] This is consistent with our synthesis conditions that the Mo : S ratio is much larger than 1 : 2. More interestingly, there is a MoS_2 nanodot decorated at the centre of the MoS_2 flake. The nanodot overall looks like pyramids. Each basal plane has a triangular shape and shrinks gradually to the summit point. Fig. 1(c) shows the cross-sectional step height profile of the MoS_2 flake along the red line indicated in Fig. 1(b). From the height profile, it can be found that the MoS_2 flake has a thickness of about 0.7 nm, which is consistent with the previous report[11] for a monolayered MoS_2 grown on the SiO_2/Si substrate. Fig. 1(d) shows the cross-sectional height profile of the pyramid-like MoS_2 nanodots decorated at the centre of the MoS_2 flake along the green dashed line indicated in Fig. 1(b). From the height profile, it can be found that the pyramid-like MoS_2 nanodot has a height of about 20 nm and a lateral size of about 1.5 μm. Fig. 1(e) shows the side view of the high resolution AFM image of a MoS_2 nanodot decorated at the centre of the MoS_2 flake. The insert is the top view of the high resolution AFM image of the pyramid-like MoS_2 nanodot. Obviously, pyramid-like features can be clearly observed as shown in the AFM images, and each basal plane has a triangular shape. The triangles stack up layer by layer and shrink gradually to the center

summit point. During the growth process of MoS_2 nanodots, the upper layers are formed later and have a shorter time to grow. Thus, the lateral layer size decreases with the height, and monolayer-by-monolayer stacked pyramid-like MoS_2 nanodots form. Fig. 1(f) shows the step height profile of the corresponding region of the side viewed MoS_2 nanodot marked by the black dotted line displayed in Fig. 1(e). The insert is the step height profile of the corresponding region of the top viewed MoS_2 nanodot marked by the blue line displayed in the inset of Fig. 1(e). The height profile shows an obvious step height of about 0.7–0.8 nm, which matches the thickness of the MoS_2 monolayer. Therefore, it can be confirmed that the pyramid-like MoS_2 nanodot is stacked with monolayer-by-monolayer MoS_2.

In order to clarify the crystal structure and quality of the pyramid-like MoS_2 nanodot decorated MoS_2 flakes, XRD measurements were performed. Fig. 2(a) shows the XRD pattern of the MoS_2 nanostructures. All the diffraction peaks in the pattern can be indexed as hexagonal-phase MoS_2 with the space group $P63/mmc$ (JCPDS no. 77-1716). No diffraction peaks from impurities are observed in the XRD pattern. From Fig. 2(a), the dominant peak reflecting the (002) plane was observed. This reflects the nature of the MoS_2 nanostructures which consist of MoS_2 layers with mostly (002) planes. Meanwhile, the very sharp peaks with high intensity and the strong (002) peak in the pattern of MoS_2 nanostructures also indicate good crystallization and a well-stacked layered structure. This result is in good agreement with the AFM observation that the nanostructured MoS_2 composed of monolayer-by-monolayer stacked pyramid-like MoS_2 nanodots on the monolayered MoS_2. Moreover, the XRD pattern is matched against a simulated XRD pattern generated by using Java Electron Microscopy Simulation (JEMS) software.[25] As shown in Fig. 2(b), the lattice constants of MoS_2 calculated from this XRD pattern are $a = b =$ 3.16 Å and c = 12.35 Å. The former is very close to the standard value of MoS_2 (a = 3.16 Å), but the latter shows an obvious increase in comparison with that of MoS_2 (c = 12.29 Å). The results indicate that the distance between neighboring MoS_2 layers increases but their in-plane structure is preserved.

The pyramid-like MoS_2 nanodot decorated MoS_2 flakes are further examined by Raman spectroscopy measurements. The solid-state excitation laser has a wavelength of 532 nm and the laser spot size was 1 μm in diameter. The Raman spectra of the monolayered MoS_2 flake region and the pyramid-like MoS_2 nanodot region are shown in Fig. 3(a) and (b), respectively. It can be found that the two characteristic Raman vibration modes E_{2g} and A_{1g} can be observed in the spectra of the monolayered MoS_2 flake and the pyramid-like MoS_2 nanodot. The E_{2g} mode is associated with the in-plane vibrations, *i.e.*, two S atoms are displaced in one direction and the Mo atom is displaced in the opposite direction. The A_{1g} mode is related to the perpendicular vibrations, *i.e.*, two S atoms are displaced in the opposite directions while the Mo atom does not move. These two Raman modes, E_{2g} and A_{1g}, exhibit a sensitive layer thickness dependence,[26] which provides a convenient and reliable means for determining the layer thickness with atomic precision. Obviously, the frequency difference between the E_{2g} and A_{1g} Raman modes is 19 cm^{-1} in Fig. 3(a) and 25 cm^{-1} in Fig. 3(b), which confirm the MoS_2 flake is monolayer and the pyramid-like MoS_2 nanodot is multilayer. This is consistent with the AFM results that the MoS_2 flake is monolayered MoS_2 and the pyramid-like MoS_2 nanodot is stacked with monolayer-by-monolayer MoS_2. As shown in Fig. 1(d) and (f), the MoS_2 nanodots are composed of a few tens of monolayers and the interlayer distance is about 0.7 nm. The effective interlayer mechanical coupling is still relatively strong, which can modify the phonon vibrations in multilayered MoS_2 nanodots. Therefore, a frequency difference of 25 cm^{-1} between the E_{2g} and A_{1g} Raman modes can be observed in the pyramid-like MoS_2 nanodot. Moreover, this frequency difference of the monolayered region suggests the good quality of the MoS_2 flake, and the frequency difference values of the pyramid-like MoS_2 nanodot indicate good preservation of the MoS_2 nanodot quality.[27] Raman mapping of the whole region further confirms the observation, as shown in Fig. 3(c) and (d). Mapping

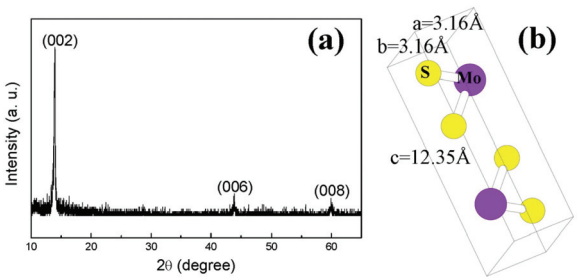

Fig. 2 (a) XRD pattern of MoS_2 flakes decorated with pyramid-like MoS_2 nanodots; (b) schematic image of MoS_2 unit cells.

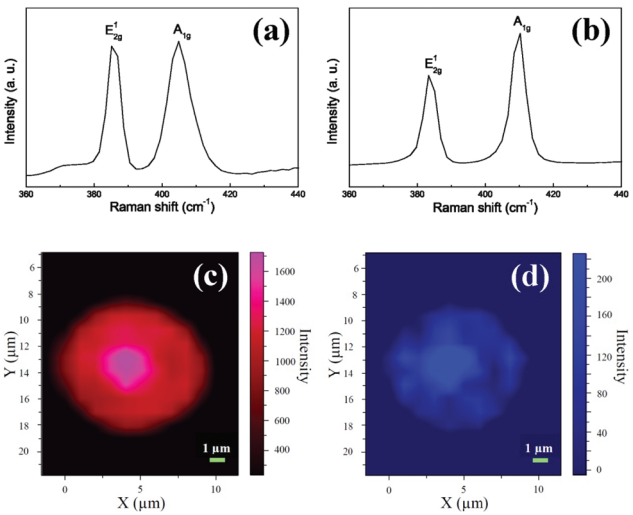

Fig. 3 (a) Raman spectra of the MoS_2 flake region; (b) Raman spectra of the pyramid-like MoS_2 nanodot region; Raman intensity mappings of (c) E_{2g} and (d) A_{1g} of the MoS_2 flakes decorated with pyramid-like MoS_2 nanodots.

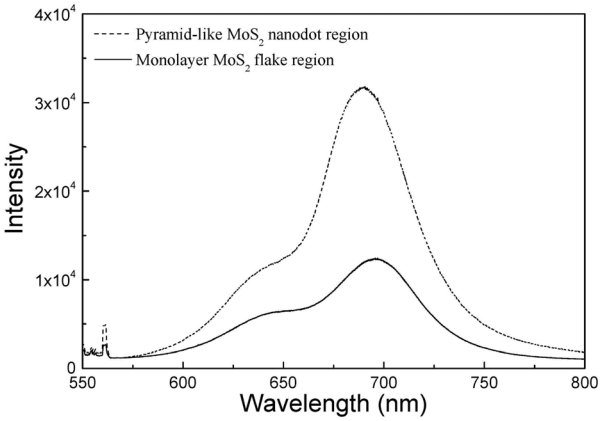

Fig. 4 PL spectra of a typical monolayered MoS_2 flake region and the pyramid-like MoS_2 nanodot region.

of the integrated intensity of the E_{2g} and A_{1g} peaks shows that the pyramid-like MoS_2 nanodot region is brighter than the monolayered MoS_2 flake region.

Fig. 4 shows the PL spectra recorded on a monolayered MoS_2 flake region and a pyramid-like MoS_2 nanodot region with a 532 nm laser source at room temperature. PL measurements were performed with the same laser excitation source and conditions as that for Raman spectroscopy. Two peaks can be observed in the PL spectra, 690 nm and 645 nm, which can be attributed to the B_1 and A_1 excitons of MoS_2, respectively.[9] Similar PL structures can be found for both the monolayered MoS_2 flake region and the pyramid-like MoS_2 nanodot region. Interestingly, in contrast to the silent PL emission of the bulk MoS_2, the PL emission of the pyramid-like MoS_2 nanodot is much stronger than that of the monolayered MoS_2 flake. It should be noted that the PL intensity of the MoS_2 nanodot is almost 3 times stronger than that of the monolayered MoS_2 flake.

To understand the PL of pyramid-like MoS_2 nanodots, we studied the electronic structural properties of MoS_2 with different phases using first-principles calculations based on density functional theory (DFT) and generalized gradient approximation (GGA). The projector augmented wave (PAW) scheme as incorporated in the Vienna ab initio simulation package (VASP) is used in the study. In addition, the van der Waals interaction between two adjacent MoS_2 layers for bulk phases is also taken into account in our calculations. The calculated energy band structures of bulk 2*H*-MoS_2, MoS_2 monolayer and bulk 1*H*-MoS_2 are shown in Fig. 5. According to Fig. 5(a) and (b), the indirect bandgap and direct bandgap for bulk 2*H*-MoS_2 and MoS_2 monolayer respectively are in good agreement with previous reports.[4,28] As we know, there is no PL for bulk 2*H*-MoS_2, which is directly related to its indirect bandgap. However, the direct bandgap results in the PL in the MoS_2 monolayer. Based on our experimental results, the pyramid-like MoS_2 nanodots have strong PL, which suggests that the pyramid-like MoS_2 nanodots should not have the stacking sequence ABAB...(2*H* phase) for MoS_2 monolayers. Therefore, we propose that the pyramid-like MoS_2 nanodots could possess the AAAA... stacking sequence (1*H* phase). In order to confirm this, we calculate the band structure (Fig. 5(c)) of bulk 1*H*-MoS_2 with the distance between two adjacent layers of 0.7 nm, which basically corresponds to the interlayer distance in our samples. It is obviously found that the bandgap is direct. A direct bandgap means the easy appearance of PL. As a consequence, the strong PL of pyramid-like MoS_2 nanodots is closely related to the stacking sequence of MoS_2 monolayers. Furthermore, due to the greater number of monolayers of pyramid-like MoS_2 structures, the PL intensity of pyramid-like MoS_2 nanodots is significantly higher than that of the MoS_2 monolayer, as observed in Fig. 4.

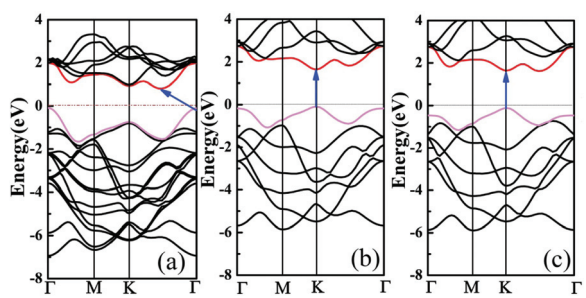

Fig. 5 Energy band structures of (a) bulk 2*H*-MoS_2; (b) MoS_2 monolayer; (c) bulk 1*H*-MoS_2.

Conclusion

In conclusion, we have demonstrated the growth of monolayer-by-monolayer stacked pyramid-like MoS_2 nanodots on monolayered MoS_2 flakes using a CVD method. Strong local PL emission has been observed for the pyramid-like MoS_2 nanostructures. First-principles calculations demonstrated that the bandgap of monolayer-by-monolayer stacked pyramid-like MoS_2 nanodots is a direct bandgap. It leads to stronger PL emission of the pyramid-like MoS_2 nanodot in comparison with that of monolayered MoS_2 flakes. The findings presented here provide new opportunities to tailor the properties of MoS_2 *via* morphology-controlled synthesis.

Acknowledgements

This work was supported by the Natural Science Foundation of China (51461019, 11164008, 51561012, 51361013 and 11264014), the Project for Young Scientist Training of Jiangxi Province (20153BCB23016) and the Natural Science Foundation of Jiangxi Province (20151BAB202004 and 20152ACB21014).

Notes and references

1 Y. Zhang, T. T. Tang, C. Girit, Z. Hao, M. C. Martin, A. Zettl, M. F. Crommie, Y. R. Shen and F. Wang, *Nature*, 2009, **459**, 820.

2 W. Z. Wu, L. Wang, Y. L. Li, F. Zhang, L. Lin, S. M. Niu, D. Chenet, X. Zhang, Y. F. Hao, T. F. Heinz, J. Hone and Z. L. Wang, *Nature*, 2014, **514**, 470.

3 A. K. Geim and I. V. Grigorieva, *Nature*, 2013, **499**, 419.

4 Q. H. Wang, K. Kalantar-Zadeh, A. Kis, J. N. Coleman and M. S. Strano, *Nat. Nanotechnol.*, 2012, **7**, 699.

5 R. Sundaram, R. Engel, A. Lombardo, R. Krupke, A. Ferrari, P. Avouris and M. Steiner, *Nano Lett.*, 2013, **13**, 1416–1421.

6 O. Lopez-Sanchez, D. Lembke, M. Kayci, A. Radenovic and A. Kis, *Nat. Nanotechnol.*, 2013, **8**, 497.

7 M. L. Tsai, S. H. Su, J. K. Chang, D. S. Tsai, C. H. Chen, C. I. Wu, L. J. Li, L. J. Chen and J. H. He, *ACS Nano*, 2014, **8**, 8317.

8 Y. J. Cao, X. F. Luo, S. M. Han, C. L. Yuan, Y. Yang, Q. L. Li, T. Yu and S. L. Ye, *Chem. Phys. Lett.*, 2015, **631–632**, 30.

9 A. Splendiani, L. Sun, Y. Zhang, T. Li, J. Kim, C. Y. Chim, G. Galli and F. Wang, *Nano Lett.*, 2010, **10**, 1271.

10 H. S. S. R. Matte, A. Gomathi, A. K. Manna, D. J. Late, R. Datta, S. K. Pati and C. N. R. Rao, *Angew. Chem., Int. Ed.*, 2010, **49**, 4059.

11 Z. Y. Zeng, Z. Y. Yin, X. Huang, H. Li, Q. Y. He, G. Lu, F. Boey and H. Zhang, *Angew. Chem., Int. Ed.*, 2011, **50**, 11093.

12 K. G. Zhou, N. N. Mao, H. X. Wang, Y. Peng and H. L. Zhang, *Angew. Chem., Int. Ed.*, 2011, **50**, 10839.

13 J. V. Lauritsen, J. Kibsgaard, S. Helveg, H. Topsoe, B. S. Clausen, E. Lagsgaard and F. Besenbacher, *Nat. Nanotechnol.*, 2007, **2**, 53.

14 Y. Y. Peng, Z. Y. Meng, C. Zhong, J. Lu, W. C. Yu, Y. B. Jia and Y. T. Qian, *Chem. Lett.*, 2001, **8**, 772.

15 C. Altavilla, M. Sarno and P. Ciambelli, *Chem. Mater.*, 2011, **23**, 3879.

16 S. Mouri, Y. Miyauchi and K. Matsuda, *Nano Lett.*, 2013, **13**, 5944.

17 K. Eshun, H. D. Xiong, S. Yu and Q. L. Li, *Solid–State Electron.*, 2015, **106**, 44.

18 T. Korn, S. Heydrich, M. Hirmer, J. Schmutzler and C. Schüller, *Appl. Phys. Lett.*, 2011, **99**, 102109.

19 A. Castellanos-Gomez, R. Roldán, E. Cappelluti, E. Buscema, F. Guinea, H. van der Zant and G. Steele, *Nano Lett.*, 2013, **13**, 5361.

20 Y. F. Chen, J. Y. Xi, D. O. Dumcenco, Z. Liu, K. Suenaga, D. Wang, Z. G. Shuai, Y. S. Huang and L. M. Xie, *ACS Nano*, 2013, **7**, 4610.

21 K. H. Liu, L. M. Zhang, T. Cao, C. H. Jin, D. N. Qiu, Q. Zhou, A. Zettl, P. D. Yang, S. G. Louie and F. Wang, *Nat. Commun.*, 2014, **5**, 4966.

22 A. R. Rezk, S. Walia, R. Ramanathan, H. Nili, J. Z. Ou, V. Bansal, J. R. Friend, M. Bhaskaran, L. Y. Yeo and S. Sriram, *Adv. Opt. Mater.*, 2015, **3**, 888.

23 B. L. Li, L. X. Chen, H. L. Zou, J. L. Lei, H. Q. Luo and N. B. Li, *Nanoscale*, 2014, **6**, 9831.

24 D. Cao, T. Shen, P. Liang, X. S. Chen and H. B. Shu, *J. Phys. Chem. C*, 2015, **119**, 4294.

25 P. A. Stadelmann, *Ultramicroscopy*, 1987, **21**, 131.

26 H. Li, Q. Zhang, C. C. R. Yap, B. K. Tay, T. H. T. Edwin, A. Olivier and D. Baillargeat, *Adv. Funct. Mater.*, 2012, **22**, 1385.

27 L. Liang and V. Meunier, *Nanoscale*, 2014, **6**, 5394.

28 W. S. Yun, S. W. Han, S. C. Hong, I. G. Kim and J. D. Lee, *Phys. Rev. B: Condens. Matter*, 2012, **85**, 033305.